

# Total neutrino and antineutrino nuclear cross sections around 1 GeV

Omair Benhar<sup>a,b</sup>, Davide Meloni<sup>a,b</sup>

<sup>a</sup>INFN, Sezione di Roma, I-00185 Roma, Italy

<sup>b</sup>Dipartimento di Fisica, Università "La Sapienza", I-00185 Roma, Italy

---

## Abstract

We investigate neutrino-nucleus interactions at energies around 1 GeV. In this regime, the main contributions to the cross sections come from quasi-elastic and production processes. Our formalism, based on the Impulse Approximation is well suited to describe both types of interactions. We focus on a series of important nuclear effects in the interaction of electron neutrinos with  $^{16}\text{O}$ , also relevant to future Beams. Our results show that the Fermi gas model, widely used in data analysis of neutrino experiments, overestimates the total cross sections by as much as 20%.

**Key words:**

**PACS:**

---

## 1 Introduction

The field of neutrino physics is rapidly developing after atmospheric and solar neutrino oscillations have been established. The results of atmospheric, solar, accelerator and reactor neutrino experiments [1] show that flavour mixing occurs not only in the hadronic sector, as it has been long known, but in the leptonic sector as well. The experimental results point to two very distinct mass differences<sup>1</sup>,  $m_{\text{sol}}^2 \approx 8.2 \times 10^5 \text{ eV}^2$  and  $m_{\text{atm}}^2 \approx 2.5 \times 10^3 \text{ eV}^2$ . Only two out of the four parameters of the three-familiy leptonic mixing matrix  $U_{\text{PMNS}}$  [4] are known:  $_{12} = 34^\circ$  and  $_{23} = 45^\circ$ . The other two parameters,  $_{13}$  and  $_{14}$ , are still unknown: for the mixing angle  $_{13}$  direct searches at reactors [5] and three-familiy global analysis of the experimental data [6,7] give the upper

---

<sup>1</sup> A third mass difference,  $m_{\text{LSND}}^2 \approx 1 \text{ eV}^2$ , suggested by the LSND experiment [2], has not been confirmed yet [3].

bound  $_{13} < 11.5$ , whereas for the leptonic CP-violating phase we have no information whatsoever. Two additional discrete unknowns are the sign of the atmospheric mass difference and the  $_{23}$ -octant (if  $_{23} \notin 45^\circ$ ).

The full understanding of the leptonic mixing matrix, together with the discrimination of the Dirac/Majorana character of neutrinos and with the measurement of their absolute mass scale, represents the main goal of neutrino physics in the next decade. The SK detector has gathered indirect evidence of  $\bar{\nu}_e$  conversion of atmospheric neutrinos whereas the SNO detector [8] has shown that a fraction of the  $\nu_e$ 's emitted by the Sun core reaches the Earth-located detectors converted into  $\nu_\mu$ 's and  $\nu_\tau$ 's (and not into unobservable sterile neutrinos). On the other hand, new-generation experiments have been proposed to look for the  $\nu_e$  mixing and intimately related parameters  $_{13}$  and  $_{23}$  through them more promising "appearance channels" such as  $\nu_e \rightarrow \nu_\mu$  (the "golden channel" [9]) and  $\nu_e \rightarrow \nu_\tau$  (the "silver channel" [10]). However, strong correlations between  $_{13}$  and  $_{23}$  and the presence of parametric degeneracies in the  $(_{13}; _{23})$  parameter space [11,12], make the simultaneous measurement of the two variables extremely difficult. A further problem arises from our present imprecise knowledge of atmospheric parameters, whose uncertainties are far too large to be neglected when looking for such tiny signals as those expected in appearance experiments [13]. Most of the proposed solutions to avoid all these problems suggest to combine different experiments and facilities, such as Super-Beams (of which T2K [14] is the first approved one),  $\bar{\nu}$ -Beams [15] or Neutrino Factories [16], although it is not completely clear whether the sensitivity of such experiments will be enough.

In view of these developments, it is vital to reduce as much as possible any source of uncertainty that could ruin the required precision and, among them, the knowledge of the neutrino-nucleus cross sections is one of the thorniest problems to be faced. In fact, the data are either very few (the case of neutrinos) or missing altogether (the case of antineutrinos). On top of that, the few available data have generally not been taken on the same targets used in the experiments (either water, iron, lead or plastics), and the extrapolation from different nuclei is complicated by nuclear effects, that can play an important role at the considered energies. Among the proposed experiments, MINER [17] and SciBooNE [18] will have the capability for precise measurements in a wide range of energies and different nuclear targets.

In this paper we will focus on total nuclear cross sections at energies up to 1 GeV, relevant to a number of neutrino experiments as well as to the planned Super-Beams and  $\bar{\nu}$ -Beams. As an example of the latter, in Fig. 1, we show the energy spectra for two different setups, in which the three decay modes of  $^{18}\text{Ne}$  [21] are considered.

In this energy regime, the dominant contribution to the charged lepton produc-

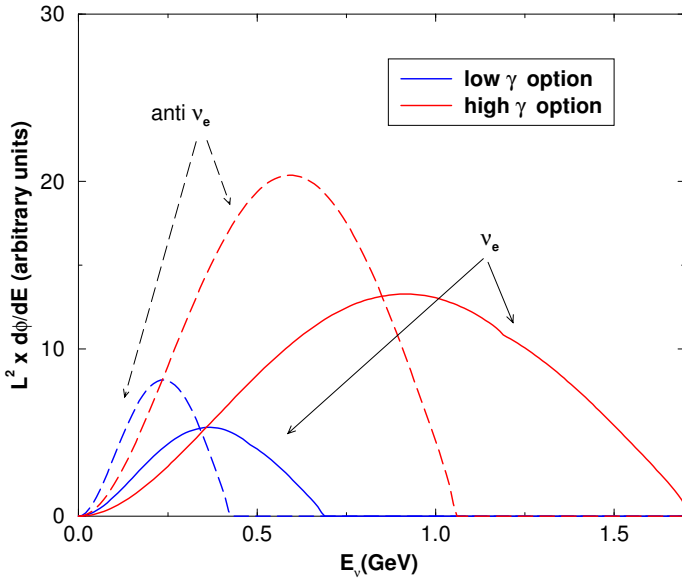


Fig. 1. Beam fluxes as a function of neutrino energy for two specific sets of values. Low and high correspond to  $(\nu_e; \bar{\nu}_e) = (100; 60)$  [19], and  $(\nu_e; \bar{\nu}_e) = (250; 150)$  [20], respectively.

tion cross section comes from quasi-elastic reactions. However, for  $E > 0.5$  GeV, inelastic production of charged leptons through excitation of the (as well as other) resonance becomes relevant. At higher energies, deep inelastic scattering also becomes progressively important, but the impact on the energy regime under investigation is expected to be negligible. Therefore, we do not take this contribution into account.

Quasi-elastic scattering, pion production and deep inelastic scattering are combined in event generators (e.g. NUANCE [22], NEUGEN [23] and NEUT [24]), that model the neutrino detector response using a simplified picture, referred to as Relativistic Fermi Gas Model (RFGM), in which the nucleus is described as a collection of quasi-free nucleons. A wealth of high-precision electron scattering data have shown that the RFGM neglects important features of nuclear dynamics [25]. The most important is the presence of strong nucleon-nucleon correlations, leading to the appearance of high momentum and high energy components in the energy-momentum distribution of the nucleons in the target nucleus [26].

In this paper we go beyond the simple RFGM, and analyse neutrino-nucleus interactions at intermediate energies using a more realistic description of nuclear dynamics, based on nuclear many-body theory (NMBT). We evaluate the cross sections for inclusive processes, in which only the outgoing charged lepton is detected, including both quasi-elastic and pion production processes. Our formalism is based on the impulse approximation (IA) picture, which is expected to be applicable at the large momentum transfers corresponding to beam energies around 1 GeV. Final state interactions (FSI) between the hadrons produced at the elementary weak interaction vertex and the specta-

tor nucleons have been not taken into account, as they do not contribute to the total cross section. However, the effect of statistical correlations between the struck nucleon and the spectators, which are known to be important in quasi-elastic scattering at low  $Q^2$ , has been included.

The plan of the paper is the following. In Section 2 we recall the formalism of the IA used to describe charged current (CC) interactions. In Section 3 we show our results for the inclusive CC cross sections, while in Section 4 we present the results for resonance production. Finally we draw the conclusions and outline the future prospects of our work. The appendices contain formulae that, together with those presented in the main text, will enable the readers to write their own codes to compute the cross sections discussed in this paper.

## 2 The Impulse Approximation

The differential cross section for the process  $\nu + A \rightarrow \nu' + X$  (Fig. 2) in which a neutrino carrying initial four-momentum  $k = (E, \mathbf{k})$  scatters on a nuclear target to a state of four-momentum  $k' = (E', \mathbf{k}')$ , the target final state being undetected, can be written in Born approximation:

$$\frac{d^2}{dE' d\Omega} = \frac{G_F^2 V_{ud}^2}{16 \pi^2} \frac{\mathbf{k}' \cdot \mathbf{j}}{|\mathbf{k}|} L \cdot W_A ; \quad (1)$$

where  $G_F$  is the Fermi constant and  $V_{ud}$  is the CKM matrix element coupling u and d quarks. The leptonic tensor, that can be written in the form

$$L = 8 \frac{h}{k^0} k^0 k + k^0 k \cdot (k^0 \mathbf{k} \cdot \mathbf{i}'' - k^0 \mathbf{k}^i) \quad (2)$$

is completely determined by lepton kinematics, whereas the nuclear tensor  $W_A$ , containing all the information on strong interactions dynamics, describes the response of the target nucleus. Its definition involves the initial and final

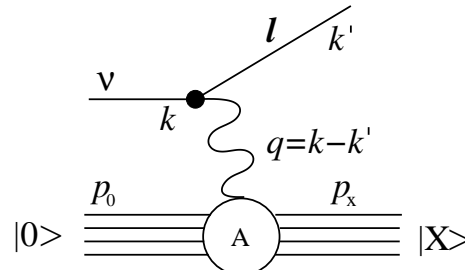


Fig. 2. Feynman diagram for the process  $\nu + A \rightarrow \nu' + X$ .

hadronic states  $\mathcal{J}i$  and  $\mathcal{J}X$ , carrying four momenta  $p_0$  and  $p_X$ , respectively, as well as the nuclear electroweak current operator  $J_A$ :

$$W_A = \sum_{X}^{X} h_0 J_A^Y \mathcal{J}X i h X J_A \mathcal{J}i \stackrel{(4)}{=} (p_0 + q - p) ; \quad (3)$$

where the sum includes all hadronic final states. Calculation of  $W_A$  at moderate momentum transfers ( $|q| < 0.5$  GeV) can be carried out within NMBT using nonrelativistic wave functions to describe the initial and final states and expanding the current operator in powers of  $q=m_N$ ,  $m_N$  being the nucleon mass. However, at higher values of  $|q|$ , corresponding to  $E > 1$  GeV, we can no longer describe the final states  $\mathcal{J}i$  in terms of nonrelativistic nucleons. Calculation of  $W_A$  in this regime requires a set of simplifying assumptions, allowing one to take into account the relativistic motion of final state particles carrying momentum  $q$ , as well as the occurrence of inelastic processes, leading to the appearance of hadrons other than protons and neutrons.

In the rest of the paper, we adopt the IA scheme, based on the assumptions that at large enough  $q$  the target nucleus is seen by the probe as a collection of individual nucleons and that the particles produced at the interaction vertex and the recoiling  $(A-1)$ -nucleon system evolve independently (see Fig. 3 for a pictorial representation of the IA picture). As a consequence, IA neglects both statistical correlations due to Pauli blocking and the rescattering processes driven by strong interactions (FSI).

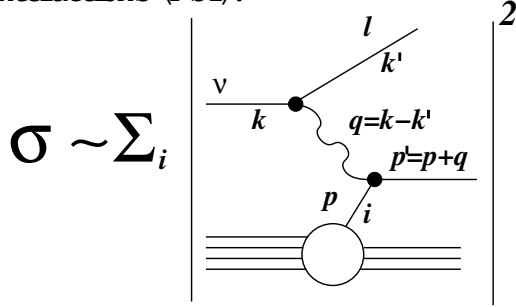


Fig. 3. Diagrammatic representation of the process  $\nu + A \rightarrow \nu + X$  in the Impulse Approximation scheme.

Within this picture, the nuclear current can be written as a sum of one-body currents, i.e.  $J_A = \sum_i J_i$ , while the final state reduces to the direct product of the hadronic state produced at the weak vertex (with momentum  $p'$ ) and that describing the  $(A-1)$ -nucleon residual system, with momentum  $p_R$ :  $\mathcal{J}i \rightarrow p'_i \mathcal{R} p_R$ . The calculation of the weak tensor is described in Ref. [27]. Here we only quote the final result:

$$W_A = \frac{G_F^2 V_{ud}^2 Z}{2} d^3 p dE P(p; E) \frac{1}{4 E_{p,j} E_{p+q,j}} W(p, q) ; \quad (4)$$

where  $E_p = \frac{q}{\vec{p}^2 + m_N^2}$ . The above definition deserves some comments. The function  $P(p;E)$  is the target spectral function, i.e. the probability distribution of finding a nucleon with momentum  $p$  and recoil energy  $E$  in the target nucleus. It then encodes all the informations about the initial (struck) particle. The quantity  $W$  is the tensor describing the weak interactions of the  $i$ -th nucleon in free space; the effect of nuclear binding of the struck nucleon is accounted for by the replacement:

$$q = ( ; q) ! \quad \bar{q} = (\bar{q}; q)$$

with  $\bar{q} = E_{p+qj} - E_{pj}$ . In particular, the variable  $\bar{q}$  takes into account the fact that a fraction of the energy transfer goes into excitation energy of the spectator system, and that the elementary scattering process can be described as if it took place in free space with energy transfer  $\bar{q} = \bar{q}$ . It follows that the second argument in the hadronic tensor is  $p = (E_{pj}; p)$ . Substituting Eq. (4) into Eq. (1), we get the final formula for the nuclear cross section:

$$\frac{d^2 \sigma_{IA}}{dE} = \int d^3p dE P(p;E) \frac{d^2 \sigma_{elem}}{dE} ; \quad (5)$$

in which we have defined the elementary cross section as

$$\frac{d^2 \sigma_{elem}}{dE} = \frac{G_F^2 V_{ud}^2}{32 \pi^2} \frac{\vec{k}^0 j}{\vec{k} j} \frac{1}{4E_p E_{p+qj}} L W : \quad (6)$$

The integration limits for Eq. (5) are given in Appendix A.

The hadronic tensor  $W$  can be written in terms of five structure functions  $W_i$  as

$$W = q W_1 + p \bar{p} \frac{W_2}{m_N^2} + i'' q p \frac{W_3}{m_N^2} + q \bar{q} \frac{W_4}{m_N^2} + (p \bar{q} + p \bar{q}) \frac{W_5}{m_N^2} : \quad (7)$$

Its contraction with the leptonic tensor (2) yields

$$L W = 16 \sum_i^X W_i \frac{A_i}{m_N^2} ! : \quad (8)$$

The functions  $A_i$ , containing kinematical factors, are collected in Appendix B whereas the structure functions  $W_i$ , expressed in terms of form factors, are

given in Appendix C.

Eq. (5) is a general formula that can be used to describe quasi-elastic scattering and resonance production in neutrino-nucleus charged current interactions. The explicit expressions differ in the analytical form of the relevant form factors and for the replacement of the energy conserving  $\delta$ -function with a Breit-Wigner factor accounting for the finite width of the resonance.

### 3 Elastic cross sections

To obtain the elastic cross sections from Eq. (5) we need to clarify the form of the structure functions  $W_i$  and the meaning of the spectral function. The first part of the job is easily done once we express the structure functions in terms of form factors  $F_1; F_2; F_A; F_P$  using the hypotheses of CVC (Conserved Vector Current) and PCAC (Partially Conserved Axial Current), as usually done for scattering on a free nucleon. In addition, the definition of the structure functions includes an energy conserving  $\delta$ -function ( $s = m_N^2$ ), where  $s = (p + q)^2$  is the squared invariant mass of the final state of the struck nucleon. In Appendix C we collect the expression of  $W_i$  in terms of form factors. Note that, except where differently stated, we use the values  $M_V = 0.84$  GeV and  $M_A = 1.05$  GeV for the vector and axial mass, respectively.

#### 3.1 Fermi gas and spectral function

The RFGM [28], widely used in Monte Carlo simulations, provides the simplest form of the spectral function:

$$P_{\text{RFGM}}(p; E) = \frac{6^{-2} A^!}{p_F^3} \delta(p_F - p) \delta(E_p - E_B + E); \quad (9)$$

where  $p_F$  is the Fermi momentum and  $E_B$  is the average binding energy, introduced to account for nuclear binding. The term in parenthesis is a constant needed to normalize the spectral function to the number of target nucleons,  $A$ . Thus, in this model  $p_F$  and  $E_B$  are two parameters that are adjusted to reproduce the experimental data. For oxygen, the analysis of electron scattering data yields  $p_F = 225$  MeV and  $E_B = 25$  MeV [29]. In more refined versions of RFGM, the binding energy of the nucleon is not a constant but a momentum-dependent function  $V(p)$  [30], entering the  $\delta$ -function in Eq. (9) according to  $(E_p + V(p) + E)$ .

Electron scattering data have provided overwhelming evidence that the energy-momentum distribution of nucleons in the nucleus is quite different from that predicted by RFGM (see, e.g. Ref. [31]). The most important feature emerged from these data is the presence of strong nucleon-nucleon (NN) correlations.

Strong dynamical correlations give rise to virtual scattering processes leading to the excitation of the participating nucleons to states of energy larger than the Fermi energy, thus depleting the single particle levels within the Fermi sea. As a consequence, the spectral function associated with nucleons belonging to correlated pairs extends to the region of  $p_j - p_F$  and  $E - E_B$ .

Clearcut evidence of correlation effects has been provided by electron- and hadron-induced nucleon knock-out experiments [32]. While the spectroscopic lines corresponding to knock out from the shell model states are clearly seen in the measured energy spectra, the associated strengths are consistently lower than expected, regardless of the nuclear mass number. Unfortunately, systematic measurements of the missing strength (typically about 20%) pushed to higher energy by NN correlations, have not been carried out yet. However, the results of a pioneering JLab experiment [33] appear to be consistent with the expectations based on lower energy data.

Correlation effects can be consistently taken into account within NMBT, in which nuclei are described in terms of nonrelativistic nucleons interacting through the hamiltonian

$$H_A = \sum_{i=1}^{A^2} \frac{p_i^2}{2m} + \sum_{j>i=1}^{A^2} v_{ij} + \dots; \quad (10)$$

where  $v_{ij}$  provides a quantitative account of the properties of the two-nucleon system, i.e. deuteron properties and 4000 accurately measured nucleon-nucleon scattering phase shifts at energies up to the pion production threshold [34], while the ellipses refer to a small additional three-nucleon potential. The energies of the ground and low-lying excited states of nuclei with mass number  $A = 10$  calculated within NMBT are in excellent agreement with the experimental values [35].

The calculation of  $P(p;E)$  within NMBT involves a degree of complexity that rapidly increases with  $A$ , so that it has been only carried out for  $A = 4$  [36,37,38,39,40,41]. However, thanks to the simplifications associated with translation invariance, highly accurate results are also available for uniform nuclear matter, i.e. in the limit  $A \rightarrow 1$  with  $Z = A/2$  [42,43] ( $Z$  denotes the number of protons).

The spectral functions for medium-heavy nuclei, ranging from Carbon ( $A = 12$ ) to Gold ( $A = 197$ ), have been modeled using the Local Density Approx-

imation (LDA) [44], in which the experimental information obtained from nucleon knock-out measurements is combined with the results of theoretical calculations of the nuclear matter  $P(p;E)$  at different densities. Within this approach,  $P(p;E)$  is divided in two parts, corresponding to low momentum nucleons, occupying shell model states, and high momentum nucleons, respectively.

The correlation contribution to  $P(p;E)$  of uniform nuclear matter has been calculated by Benhar et al. for a wide range of density values [44]. Within the LDA scheme, the results of Ref. [44] can be used to obtain the corresponding quantity for a finite nucleus of mass number  $A$ . The full LDA nuclear spectral function can then be written as

$$P_{\text{LDA}}(p;E) = P_{\text{MF}}(p;E) + P_{\text{corr}}(p;E) : \quad (11)$$

From the spectral function, we can obtain the nucleon momentum distribution, defined as

$$n(p) = \int_0^Z dE P(p;E) : \quad (12)$$

The nucleon momentum distributions of  $^{16}\text{O}$  and  $^{197}\text{Au}$  obtained from LDA, normalized to unity, are shown in Fig. 4. For reference, the RFGM momentum distribution corresponding to Fermi momentum  $p_F = 225 \text{ MeV}$  is also shown by the dashed line.

The results of Fig. 4 show that  $n(p)=A$  becomes nearly independent of  $A$  at large  $p \gtrsim 300 \text{ MeV}/c$ . This feature suggests that the correlation part of the spectral function also scales with the target mass number, so that nuclear matter results can be used at finite  $A$ . It also clearly appears that the LDA  $n(p)$  is very different from that obtained from the RFGM, in which the large momentum tail is missing.

As pointed out in Section 1, within IA allFSI, which are long known to be important in semi-inclusive and exclusive electron-nucleus scattering processes, are neglected. In quasi-elastic inclusive processes dynamical FSI are much weaker, their main effects being i) an energy shift of the differential cross section, due to the fact that the struck nucleon feels the mean field generated by the spectator particles and ii) a redistribution of the strength, leading to the quenching of the peak and the enhancement of the tails. As a consequence, FSI do not affect the total inclusive cross section, resulting from integration over the lepton variables (energy loss and scattering angle), and therefore will not be taken into account in our work.

On the other hand, statistical correlations, leading to Pauli blocking of the

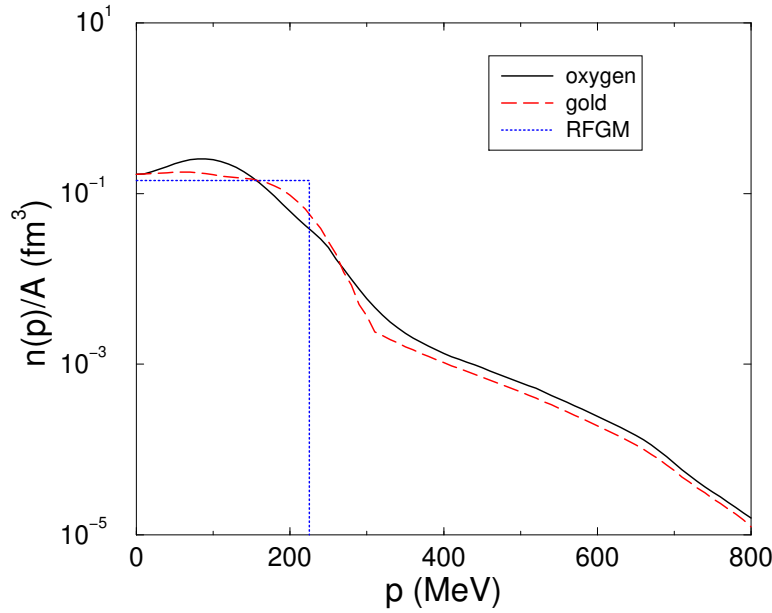


Fig. 4. Momentum distribution of nucleons in the oxygen (solid line) and gold (dotted line) ground states. Dashed line: RFGM with Fermi momentum  $p_F = 225$  MeV and  $E_B = 25$  MeV.

phase space available to the knocked-out nucleon, need to be included. A rather crude prescription to estimate their effects amounts to modifying the spectral function through the replacement

$$P(p; E) \rightarrow P(p; E) \left( \frac{p}{p_F} + q_j \right) \quad (13)$$

where  $\bar{p}_F$  is the average nuclear Fermi momentum, defined as

$$\bar{p}_F = \frac{1}{Z} \int d^3r \rho_A(r) p_F(r); \quad (14)$$

with  $p_F(r) = (3^2 \rho_A(r) - 2)^{1/3}$ ,  $\rho_A(r)$  being the nuclear density distribution. For oxygen, Eq. (14) yields  $\bar{p}_F = 209$  MeV. Note that, unlike the spectral function, the quantity defined in Eq. (13) does not describe intrinsic properties of the target only, as it depends explicitly on the momentum transfer. Overall, the approach described above involves no adjustable parameters (as compared with other models discussed in Section 3.2).

The relative weight of different nuclear effects is illustrated in Fig. 5, showing the total cross section of the process  $e + {}^{16}\text{O} \rightarrow e + X$  as a function of neutrino energy. The dot-dash line represents eight times the elementary cross section, i.e. the cross section for interactions of neutrinos on free neutrons. The dashed line is the result of the RFGM without inclusion of Pauli blocking (PB). The difference between the dot-dash and dashed lines, the latter being sizably

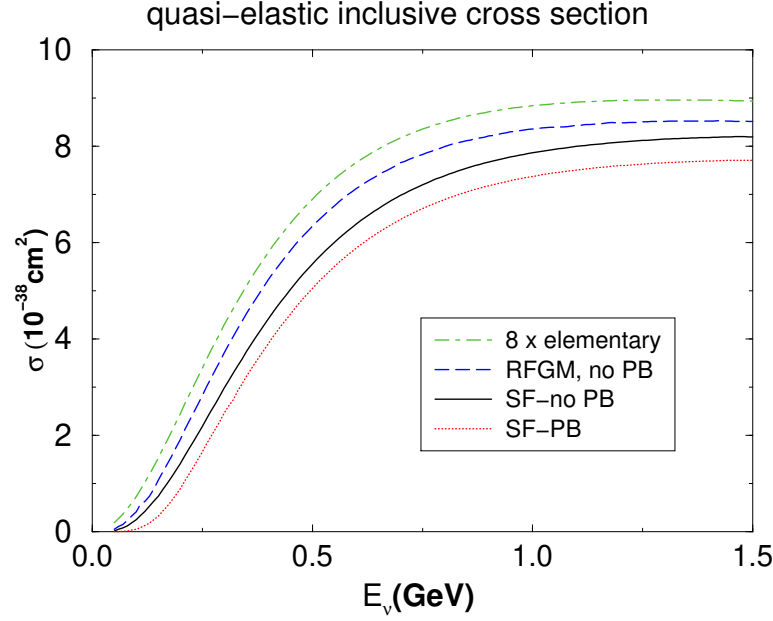


Fig. 5. Total quasi-elastic cross section for the process  $e^{16}\text{O} + e \rightarrow X$ . The dot-dash line represents eight times the elementary cross section; the dashed line is the result of the RFGM with Fermi momentum  $p_F = 225$  MeV and binding energy  $E_B = 25$  MeV; the dotted and solid lines have been obtained using the LDA spectral function, with and without inclusion of Pauli blocking, respectively.

smaller, results from the Fermi motion (with momenta not exceeding  $p_F$ ) of the target nucleons. The solid line corresponds to our results obtained from the LDA oxygen spectral function. It clearly appears that the inclusion of NN correlations leads to a further reduction of the cross section. This reduction is further enhanced if we include PB, as shown by the dotted line, since the available phase space for the knocked nucleon gets smaller, see Eq. (13). Note that, as expected, the importance of PB decreases as neutrino energy increases. For example, the difference between the solid and dotted lines turns out to be 10 % and 6 % at neutrino energy 0.5 GeV and 1.5 GeV, respectively. It has to be mentioned that the prescription of Eq.(13) can also be used to include PB in the RFGM. The size of the effect is the same as in the calculation using the spectral function, the resulting cross section being suppressed by 5–10 % with respect to the dashed line of Fig. 5. Overall, based on the results shown in Fig. 5 one can safely state that a realistic treatment of neutrino-nucleus interactions must go beyond the RFGM.

The same conclusions can be drawn for antineutrino interactions. Neglecting the isospin breaking effect leading to the proton to neutron mass difference, the same Eqs. (5)–(6) can be applied. The only difference arises in the sign in front of the parity-violating term of Eq. (7), “+”, which should be replaced by “−”. Therefore, we do not show the corresponding figure.

### 3.2 Comparison with other models

Over the past few years, many authors have investigated neutrino cross sections and the related nuclear effects (see, e.g., Ref. [45]). In this section we compare our results with the existing literature for the case of oxygen and carbon targets. It has to be kept in mind, however, that, while many of the available results correspond to  $E < 100$  MeV [46], the IA scheme adopted in our work is not expected to be accurate in this regime. Therefore, our comparison is mostly focused on the region of higher energies.

In Ref.[47], the CC quasielastic cross section is obtained from the self-energy of the gauge bosons  $W$  in the nuclear medium, whose calculation is carried out using the medium-modified nucleon propagator resulting from a LDA implementation of the Fermi gas model. The effects of long range nuclear correlation (RPA) are also included by means of an effective NN interaction of the Landau-Migdal type. Coulomb distortion effects, accounting for the fact that the charged lepton produced in neutrino interaction is moving in the Coulomb field of the nucleus, are also taken into account. A collection of the resulting  $^{16}\text{O} (e; e)X$  is reported in Tab. IV of Ref. [47], in which relativistic and non-relativistic nucleon kinematics, as well as the inclusion of FSI and RPA effects are analyzed.

In Fig. 6 we compare our results to those of Ref. [47]. The solid line corresponds to our calculation with the LDA spectral function and PB included; the shaded area is bounded by the minimum and maximum values of the cross section

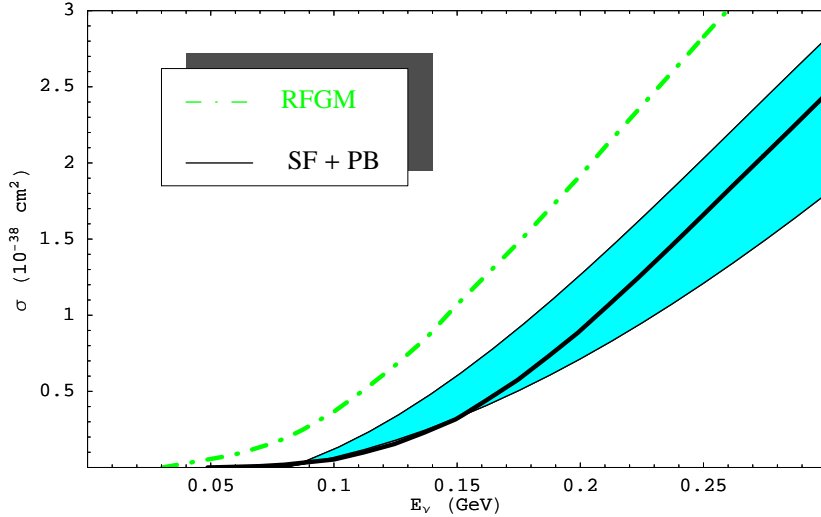


Fig. 6. Comparison between our results for  $^{16}\text{O} (e; e)X$  (solid line) and those presented in [47]; the shaded region represents the range of cross sections predicted in Ref.[47] (see text for details). The RFGM results corresponding to Fermion momentum  $p_F = 225$  MeV and  $E_B = 25$  MeV are also shown.

of Ref.[47]. For reference, the RFGM prediction is also included. It can be seen that the agreement between our results and those reported in Ref.[47] is satisfactory. The small discrepancy at low neutrino energy, below 0.15 GeV, is likely to be ascribed to the inadequacy of the IA to describe small momentum transfer processes. It is apparent that the RFGM largely overestimates the cross section.

At higher energies, we compare our results with those of Refs.[48] and [49]. In the first paper,  $(^{16}\text{O} (e; e) X)$  is calculated using the same formalism as described in [47]. The corresponding results are presented in the top panel of Fig. 7.

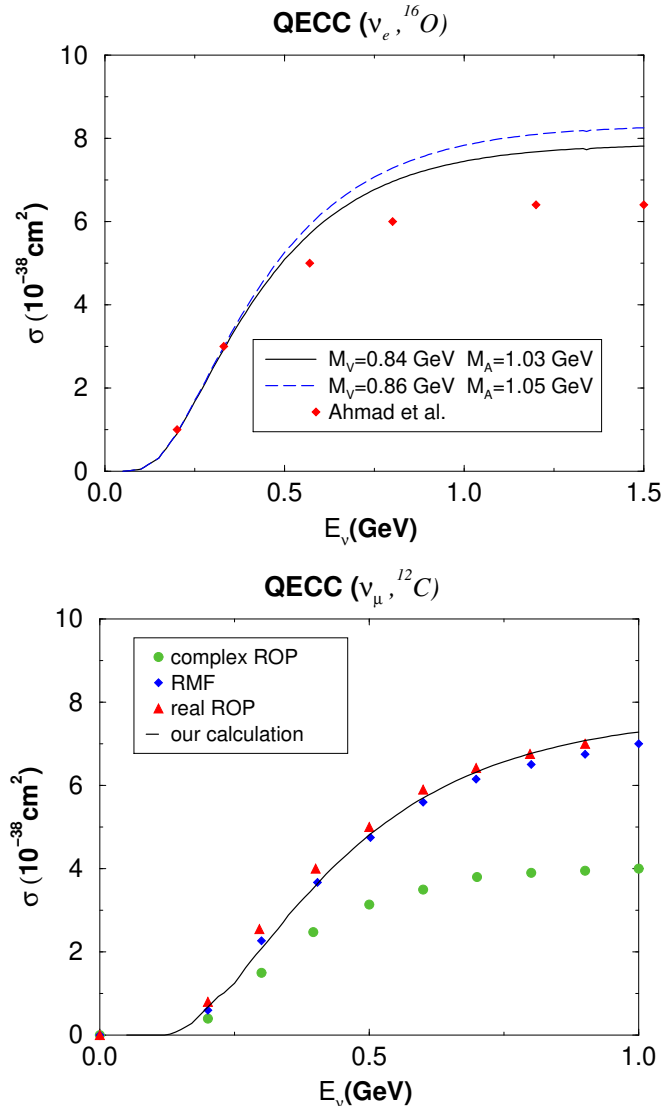


Fig. 7. Top: comparison between  $(^{16}\text{O} (e; e) X)$  resulting from our calculations (solid and dashed lines) and that of Ref.[48]. Bottom: comparison of  $(^{12}\text{C} ( ; ) X)$  resulting from our calculations and those obtained in Ref.[49] using different models (see text for details).

In order to pin down the source of the sizable disagreement between our results and those of Ref.[48], we have tested the sensitivity of the cross section to the vector and axial masses using two different sets of values:  $M_V = 0.86$  and  $M_A = 1.05$ , as employed by Ahmadi et al. [48], and  $M_V = 0.84$  and  $M_A = 1.03$ . It clearly appears that the discrepancies at  $E > 0.5$  GeV cannot be removed by a different choice of  $M_V$  and  $M_A$ , and should rather be ascribed to the different descriptions of nuclear dynamics.

A much better agreement is observed in the bottom panel of Fig. 7, in which we compare our results for  $^{12}\text{C}(\text{; } \text{; })\text{X}$ , to those obtained in Ref.[49] using different models. The approach of Mairon et al., based on a IA scheme similar to the one adopted in our work, uses Relativistic Shell-Model wave functions to describe bound nucleon states and two different prescriptions to include FSI effects. The final state of the knocked out nucleon is described using i) distorted waves obtained solving the Dirac equation with a phenomenological relativistic complex optical potential (ROP) or ii) the continuum solutions of the same Dirac equation used for the initial bound states (Relativistic Mean Field (RMF) approach.

The diamonds in the bottom panel of Fig. 7 show the RMF results of Ref. [49], whereas triangles-up and circles have been obtained by the same authors including the real part only and the full ROP (real + imaginary part), respectively. The most striking feature is the large effect of the imaginary part of the ROP, leading to a suppression of the total cross section of more than 40 %. This effect can be easily understood, as the imaginary optical potential produces a loss of flux in the one particle-one hole channel. However, it contradicts the well known result stating that, in the kinematical regime in which incoherent scattering dominates, the integrated inclusive cross section is not affected by FSI [50]. In fact, it has long been realized that, unless the reappearance of the missing flux in the two particle-two hole channel is properly taken into account, the prescription employed in Ref. [49] leads to a violation of the non energy weighted sum rule of the nuclear response [50]. On the other hand, Fig. 7 shows that the cross sections obtained by Mairon et al. neglecting FSI effects or using only the real part of the ROP, whose effect is very small, are in excellent agreement with our results.

#### 4 Inelastic cross sections

One pion production is the second process which contributes to the total cross section in the kinematical regime discussed in this paper; it proceeds mainly through resonance production, the leading contribution coming from

excitation of the , i.e. through the the processes

$$\gamma + n \rightarrow \pi^+ + \gamma; \quad \gamma + p \rightarrow \pi^+ + \pi^0; \quad (15)$$

In this section, we calculate the inclusive resonance production cross section applying the same formalism used for quasi-elastic interactions, in which nuclear effects in the initial state are described by the spectral function. Obviously, PB has no impact on the produced at the weak interaction vertex, although it may affect the phase space available to the nucleon appearing in the aftermath of its decay. It has to be kept in mind, however, that the inclusive cross section is only sensitive to processes taking place within a distance  $1 = \gamma \gamma j$  of the primary vertex, so that at large enough  $\gamma \gamma j$  it is unlikely to be affected by two-step reaction mechanisms.

#### 4.1 resonance production

To account for production, we can apply Eqs. (5)–(8) with only minor changes. Unlike the quasi-elastic case, the structure functions depend now on two variables, namely  $Q^2$  and  $W^2$ , where  $W^2$  is the squared hadronic invariant mass. The energy conserving  $\gamma$ -function is replaced by the Breit-Wigner factor

$$\frac{M_R}{(W^2 - M_R^2)^2 + M_R^2 \Gamma_R^2}; \quad (16)$$

where  $M_R$  is the resonance mass and  $\Gamma_R$  its decay width, and an additional integration in the variable  $W$  must be carried out. For the dependence of the structure functions on form factors for  $\pi^+$  production, we closely follow Ref. [51]<sup>2</sup> and use isospin symmetry to relate  $\pi^+$  and  $\pi^0$  form factors through

$$h^{\pi^+} \gamma^A \gamma^\mu = \frac{p}{3} h^{\pi^0} \gamma^A \gamma^\mu; \quad (17)$$

It has to be mentioned that, in principle, the form factors entering the calculation of the cross section could be extracted from proton and deuteron data. However, electron scattering studies show that extrapolations of the existing phenomenological models to the region of low  $Q^2$  leads to sizably underestimate the nuclear cross sections in the production region [27,52].

Our results for CC production via  $^{16}\text{O}(\gamma; e)$  interactions are shown in Fig. 8, and compared with the elementary cross section and the RFGM prediction.

<sup>2</sup> Notice that, compared to Eq. (7), the parametrization of the hadronic tensor in [51] involves an additional factor  $1/2$  in the coefficient of  $W^3$ .

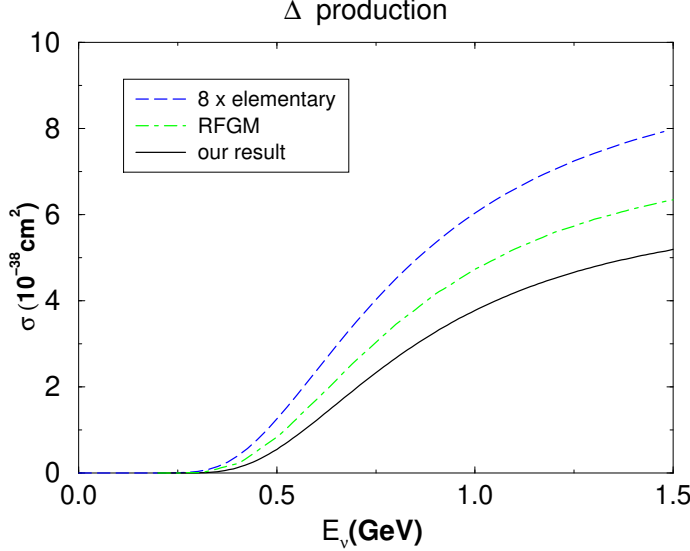


Fig. 8. CC production via  $^{16}\text{O} (e;e)$  interactions. The solid line shows the results obtained using the LDA spectral function; the dashed and dot-dash curves are the elementary cross section and the RFGM prediction (with  $p_F = 225$  MeV and  $E_B = 25$  MeV), respectively.

As in the elastic case, nuclear effects strongly reduce the cross section with respect to the free space value; moreover, the RFGM appears to overestimate production, an effect that has been already observed by different authors (see, e.g., [53,54]).

Fig. 9 illustrates the relative weight of the quasi-elastic and  $\Delta$  production channels in the total inclusive  $^{16}\text{O} (e;e)$  cross section.

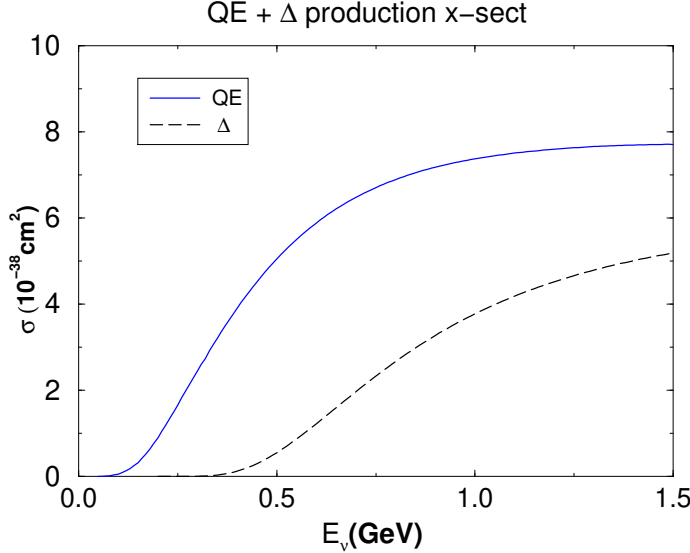


Fig. 9. Comparison between the CC quasi-elastic (solid line) and  $\Delta$  production (dashed line) contributions to the total cross section of the process  $^{16}\text{O} (e;e)$ .

Above  $E = 0.5$  GeV, the production contribution becomes important; in particular, the ratio of the areas under the curves is of the order of 40 %, thus showing the importance of including such a contribution in realistic estimates of the cross sections. To gauge the impact of production on the measurements at -Beam s, we have computed the averaged cross section

$$h_i(\gamma) = \frac{\int_0^R dE \frac{d\sigma_{\text{QE}}(E; \gamma)}{dE} \frac{d\sigma_i(E)}{dE}}{\int_0^R dE \frac{d\sigma_{\text{QE}}(E; \gamma)}{dE}} \quad i = \text{QE}; \quad (18)$$

for the fluxes reported in Ref.[20], and constructed the ratio  $h_i = h_{\text{QE}} i$  as a function of the boost factor  $\gamma$ . The results are shown in Fig. 10.

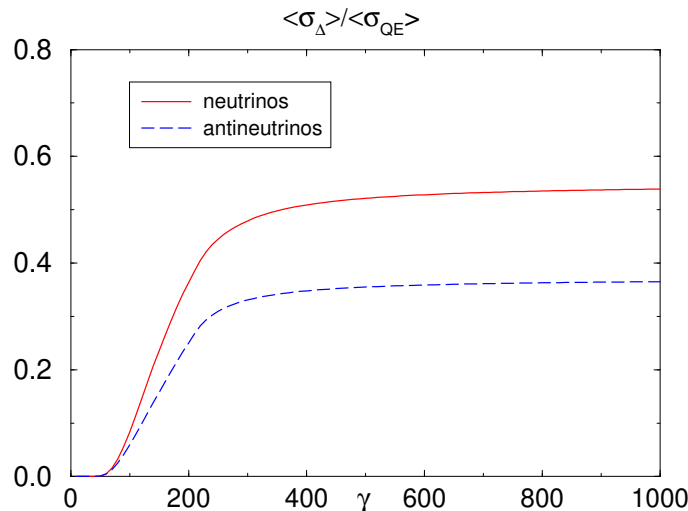


Fig. 10. Ratio  $h_i = h_{\text{QE}} i$  as a function of the boost factor  $\gamma$  at -Beam s. The solid (dashed) line refers to neutrino (antineutrino).

It clearly appears that the ratio of  $h_i$ 's becomes larger and larger as the factor increases, until it becomes quite stable at  $\gamma > 600$  reaching the values 0.52 and 0.37 for neutrino and antineutrino, respectively. This implies that the production contribution to the total cross section is about 1=2 or 1=3 of the main contribution from CC quasi-elastic interactions. The presence of the plateaux is due to the fact that at higher energies the cross sections exhibit almost the same energy dependence. Comparing with Fig. 1 we also understand the reason why the production process contributes more to neutrino than to antineutrino cross section. For fixed  $\gamma$ , the antineutrino spectra is peaked at lower energies than the neutrino one, in a region where the contribution of the  $\Delta$  is less important. In Appendix D we list separately the values of  $h_{\text{QE}} i$  and  $h_i$  for the spectra of Fig. 1.

## 4.2 Contribution of higher resonances

Beside the contribution of the  $\Delta$  to the inelastic cross section, other resonances may be important, particularly for neutrino energies larger than 2 GeV. This so-called second resonance region contains three isospin 1/2 states:  $P_{11}$  (1440);  $D_{13}$  (1520);  $S_{11}$  (1535). New data on electroproduction have enabled the authors of [55] to estimate the vector form factors of these resonances. On the other hand, estimates for the axial couplings have been obtained from the decay rates of the resonances, exploiting the PCAC hypothesis. The strategy for computing their contributions to the cross section is the same used for production, and we refer to [55] for a compilation of the form factors. Our results are shown in Fig. 11.

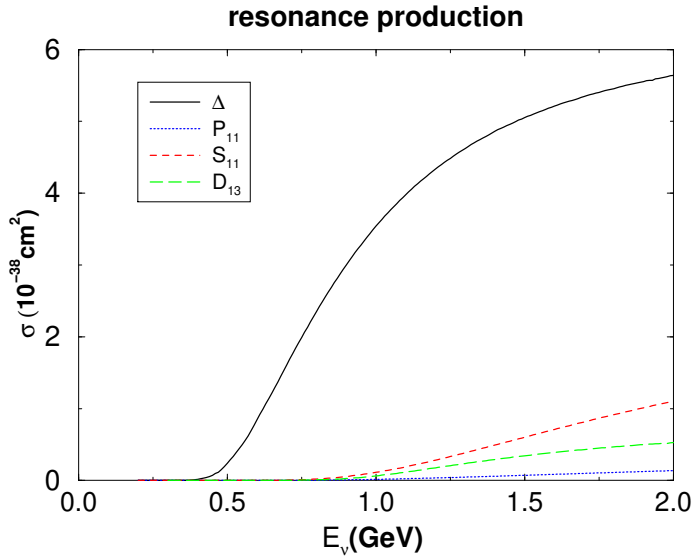


Fig. 11. CC resonance production via  $^{16}\text{O} (e; e)$  interactions. The solid line shows the results for the  $\Delta$  production, whereas the long dashed, dashed and dotted lines correspond to  $D_{13}$ ,  $S_{11}$  and  $P_{11}$ , respectively.

As expected, even at the end of the energy spectra of Fig. 1, the contribution of the second resonance turns out to be marginal. For example, at  $E = 1.5$  GeV, the ratio of the cross sections is  $S_{11} : D_{13} : P_{11} = 1 : 0.12 : 0.06 : 0.02$ .

## 4.3 Comparison with other calculation and experimental data

As for the quasi-elastic case, many papers have been devoted to the subject of resonance production. However, most of them focus on exclusive channels (a subject only marginally addressed in the following) and consider targets other than oxygen or carbon [56,57]. For the sake of completeness, in Fig. 12 we compare our calculation for production in  $^{16}\text{O} (e; e)$  interactions to the

results of Ref. [48]. The agreement between the two calculations appears to be reasonable, for both neutrino and antineutrino production.

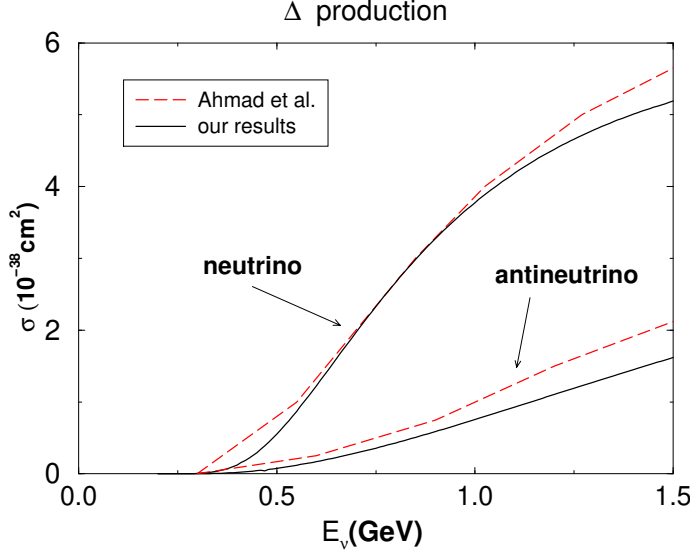


Fig. 12. Comparison of our cross sections (solid lines) for  $^{16}\text{O} (e;e^-)$  and  $^{16}\text{O} (e;e^+)$  to those of Ref. [48] (dashed lines).

To end this section, we compare our calculations to the preliminary results of the MINIBOON E collaboration for the cross section of the CC process  $\text{e} + ^{12}\text{C} \rightarrow \text{e} + \text{X}$  [58].

We should mention that a complete treatment of exclusive channels has not been carried out yet within our formalism. In particular, we are able to estimate incoherent  $\pi^+$  production (in which the target nucleus can be excited and/or broken up, leading to the production of pions) whereas we have not taken into account the production channel  $\text{e} + \text{A} \rightarrow \text{e} + \text{A} + \pi^+$ , in which the target nucleus is left in the ground state (coherent pion production).

As the CC one  $\pi^+$  production cross section is extracted from the measured ratio

$$R = \frac{\sigma_{\text{CCQE}}^+}{\sigma_{\text{CCQE}}} \quad (19)$$

using a specific model for CC quasi-elastic cross section, we prefer to calculate  $R$  from our model and then compare directly with Fig. 5 of [58]. We also include the contribution of the second resonance region.

The following isospin decomposition can be applied to the pion production amplitudes  $A$  [57]

$$A(\text{e} + \text{p} \rightarrow \text{e} + \text{p} + \pi^+) = A_3;$$

$$\begin{aligned}
A(\pi^+ + n \rightarrow \pi^+ + n + \Delta^0) &= \frac{1}{3}A_3 + \frac{2}{3}A_1; \\
A(\pi^+ + n \rightarrow \pi^+ + p + \Delta^0) &= \frac{2}{3}A_3 + \frac{2}{3}A_1;
\end{aligned} \tag{20}$$

where  $A_3$  is the amplitude for the isospin 3=2 state of the  $N$  system, predominantly the  $\Delta$ , and  $A_1$  is the amplitude for the isospin 1=2 state. From the above decomposition, we obtain the  $\pi^+$  production cross section

$$(\pi^+ + p \rightarrow \pi^+) = \frac{10}{9}(\pi^+ + \Delta^0) + \frac{8}{9}(b_1 P_{11} + b_2 D_{13} + b_3 S_{11}); \tag{21}$$

where the coefficients  $b_i$  are branching ratios for  $\Delta^0$  production of the resonances (which we assume to be equal to 0.7 for  $P_{11}$ ,  $D_{13}$  and  $S_{11}$ ).

The results of the calculation are shown in Fig. (13) in which the experimental points are taken from [58]; the dashed line refers to the contribution only, whereas the solid line is obtained using Eq. (21).

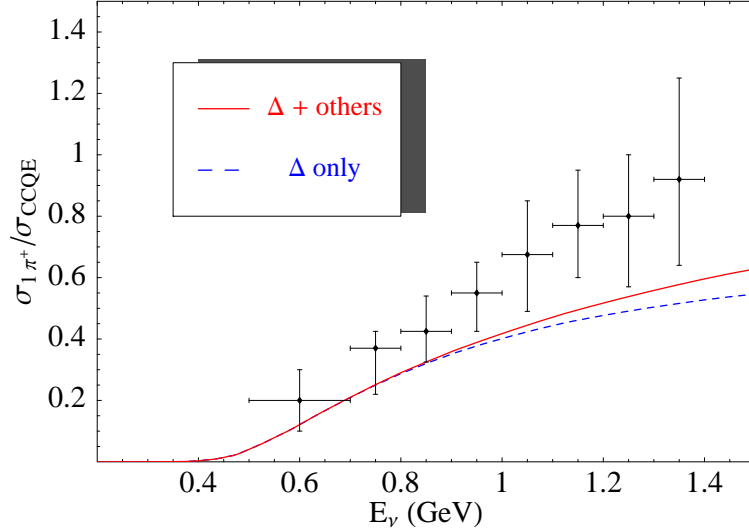


Fig. 13. Comparison between the preliminary MiniBooNE data for the ratio  $R = \sigma_{\pi^+ + p} / \sigma_{\text{CCQE}}$  in the process  $\nu + {}^{12}\text{C} \rightarrow \pi^+ + \Delta^0 + X$  and the results of our calculation. The dashed line refers to the contribution only, whereas the solid line is obtained considering also the contribution from the second resonance region (see Eq. (21)).

The figure shows a fair agreement between experiment and theory. However, at energies above  $E \approx 1$  GeV our curves are below the data. This may be ascribed to non-resonant pion production [59] which has not been taken into account in the calculation. Another 10% contribution could also come from coherent pion production [58]. A fully quantitative understanding of these effects deserves further studies.

## 5 Conclusions

In this paper we have investigated neutrino interactions with nuclei at energies up to  $1 \text{ GeV}$ . In this energy region, the main contributions to the total inclusive cross section come from CC quasi-elastic and resonance production processes. To estimate the cross sections, we employed a formalism based on IA, applicable to both quasi-elastic and inelastic processes.

For the quasi-elastic  ${}^{16}\text{O} (e; e')$  interactions, we compare various theoretical models, based on different descriptions of nuclear dynamics. We find that the simple RFGM overestimates the cross sections, with respect to the results obtained using a realistic spectral function to describe the strongly correlated bound nucleons. While dynamical FSI play no role in the total inclusive cross section, statistical correlations, arising from the effect of Pauli principle, further decrease the cross section, as the phase space available to the knocked out nucleons is reduced. Therefore, our best estimate of the inclusive total cross section is obtained using the LDA spectral function and including Pauli blocking. These results are in fair agreement with those discussed in the existing literature.

Although the formalism we have employed can be readily applied to a variety of different targets, for which realistic spectral functions are available, most of the available quasi-elastic neutrino data have been taken at low energies, where IA is not expected to provide accurate predictions. Higher energy data will soon be provided by K2K SciBar experiment [60] and MinerA [17].

As for the inelastic cross sections, we focused on resonance production, including the contribution of both the and the second resonance region. The calculated inclusive resonance production cross sections show that, as in the elastic case, the simple RFGM appears to be unable to accurately describe these processes. As expected, the CC resonance production to quasi-elastic cross section ratio becomes increasingly important at  $E > 0.5 \text{ GeV}$ . At energies below  $E = 2 \text{ GeV}$ , the contribution of  $P_{11}; D_{13}$  and  $S_{11}$  to the total cross section turns out to be small, being  $\sim 10\%$ .

Even if we do not consider exclusive channels explicitly, we provide an estimate of the one  $\pi^+$  production through resonance excitation. Comparison between the calculated ratio  $R = \frac{\pi^+}{\pi^+ + \text{CCQE}}$  to the preliminary results from the MINIBoNE collaboration shows a fair agreement between theory and data at  $E < 1 \text{ GeV}$ . On the other hand, at higher energies, a discrepancy emerges that may be removed once the contributions of non-resonant and coherent pion production are properly added to our results.

## Acknowledgments

The authors are indebted to P. Lipari for a critical reading of the manuscript. D. M. wishes to thank J.J. Gomez Cadenas, M. Sorel, G.P. Zeller and M. Wascko for illuminating discussions on the status of the K2K and MINIBoONE cross section determination. Many discussions with O. Lalakulich, M. Lusignoli and M. Sakuda are also gratefully acknowledged.

## A Integration limits

Let us analyze in detail the integration limits involved in the calculation of the quasi-elastic and anelastic cross sections. The integration momentum in Eq. (5) can be cast in the form

$$d^3p = p^2 dp d\cos\theta ; \quad (A.1)$$

where  $\theta$  is the angle between  $p$  and  $q$  and the integral on the azimuthal angle can be readily done, yielding a factor 2. Denoting by  $W$  the invariant mass of the final hadronic state produced in the interaction,  $\cos\theta$  can be written in the form :

$$\cos\theta = \frac{W^2 - \vec{p}\vec{j} - \vec{q}\vec{j} + (\gamma + E_p)^2}{2\vec{p}\vec{j}\vec{q}\vec{j}} ;$$

or, equivalently,

$$\cos\theta = \frac{s + M_{A-1}^2 - W^2 - 2(\gamma + M_A)E_{A-1}}{2\vec{p}\vec{j}\vec{q}\vec{j}} ; \quad (A.2)$$

where  $M_{A-1} = M_A - m_N + E$ ,  $s$  is the squared center of mass energy and  $E_{A-1}^2 = M_{A-1}^2 + \vec{p}\vec{j}$ . The quantity  $\cos\theta$  has to satisfy the constraints  $-1 \leq \cos\theta \leq 1$ , leading to the lower and upper bounds for  $\vec{p}\vec{j}$ :

$$\vec{p}\vec{j} = \frac{1}{2s} (\vec{q}\vec{j} - (\gamma + M_A)^2)^{1/2} - 4sM_{A-1}^{1/2} ; \quad (A.3)$$

with  $\gamma = s + M_{A-1}^2 - W^2$ . The upper limit of the  $E$  integration can be found requiring the argument of the square root entering the definition of  $\vec{p}\vec{j}$  to be non-negative. This leads to  $\sqrt{s}M_{A-1}$  and finally to the bound

$$E_{max} = \frac{p}{s} (M_A - (W - m_N)) ; \quad (A.4)$$

### A .1 Quasi-elastic case

Up to now the integration limits we have found are completely general. The quasi-elastic case is recovered once we put  $W = m_N$ . Equation (5) can be cast in a simpler form once we use the energy conserving  $\delta$ -function to perform the integration on  $\cos \theta$  in Eq. (A.1). We have to evaluate the Jacobian of the transformation

$$\frac{\partial}{\partial \cos \theta} (s - m_N^2) = 2 \vec{p}_j \vec{p}_j;$$

leading to the final formula

$$\frac{d^2 \sigma_{IA}}{d dE} = \frac{2}{\vec{p}_j} \int_0^Z dp dE \vec{p}_j \vec{p}_j P(p; E) \frac{d^2 \sigma_{elem}}{d dE}; \quad (A.5)$$

### A .2 Resonance production

For the case of resonance production, the variable  $W$  is the invariant mass of the resonance. It is more convenient to express Eq. (A.1) in terms of  $\vec{p}_j$  and  $W$  instead of  $\vec{p}_j$  and  $\cos \theta$ . It can be easily done with the help of Eq. (A.2), implying

$$d^3 p = p^2 dp d\cos \theta \frac{2}{\vec{p}_j} W dW \vec{p}_j dp; \quad (A.6)$$

The cross section for resonance production can then be written in the following form :

$$\frac{d^2 \sigma_{IA}}{d dE} = \frac{2}{\vec{p}_j} \int_{W_{th}}^{W_{Z^* ax}} \frac{Z^*}{W} dW \int_p^{\frac{Z^*}{W}} \vec{p}_j dp \int_0^{E_{Z^* ax}} dE P(p; E) \frac{d^2 \sigma_{elem}}{d dE}; \quad (A.7)$$

where  $d^2 \sigma_{elem} = d dE$  has the same form as in Eq. (6) but the hadronic tensor involves the Breit-Wigner factor of Eq. (16) and the structure functions are those specified in Ref. [51].

## B Kinematical factors

Here we report the kinematical factors appearing in the general formula for the cross sections, after tensor contraction (Eq. (6)):

$$\begin{aligned}
 A_1 &= m_N^2 (k^0 \bar{k}^0) \\
 A_2 &= (k^0 \bar{p}) (k^0 \bar{p}) \frac{A_1}{2} \\
 A_3 &= (k^0 \bar{p}) (k^0 \bar{q}) (k^0 \bar{q}) (k \bar{p}) \\
 A_4 &= (k^0 \bar{q}) (k^0 \bar{q}) \frac{q^2}{2} \frac{A_1}{m_N^2} \\
 A_5 &= (k^0 \bar{p}) (k^0 \bar{q}) + (k^0 \bar{p}) (k^0 \bar{q}) \left( \frac{A_1}{m_N^2} \bar{p} \right);
 \end{aligned} \tag{B.1}$$

where

$$k = (E; k) \quad k^0 = (E^0; k^0)$$

$$p = (E_p; p) \quad q = (\bar{q}; q) :$$

Notice that, due to the symmetry of the problem, some of the scalar products considerably simplify. In fact, using a reference system in which the vector  $q$  is along the  $z$ -axis and scattering takes place in the  $xz$ -plane, one can express the scalar products in terms of momentum component in that plane and, using the symmetry of the problem, neglect terms linear in  $p_x$ . The evaluation of the remaining contributions is straightforward.

In the limit in which  $q \neq q$  and  $p \neq p$ , the coefficients  $A_{2,5}$  reduce to kinematical factors of free elastic interactions. In particular,  $A_{4,5}$  depend linearly on the lepton mass, thus vanishing in the limit of massless leptons. This is no longer true in our formalism, in which, even in the limit of massless leptons,  $A_{4,5}$  are different from zero. The relative contribution of each term appearing in Eq. (8) is shown in Fig. B.1 in which we plot the quasi-elastic cross section for electron neutrinos on  $^{16}\text{O}$ .

While the main contributions come from  $A_{1,3}$ , non-vanishing  $A_{4,5}$  give an additional 4% to the cross section. For heavier lepton masses, the contribution of  $A_{4,5}$  is increasingly larger, as expected for free nucleon interactions.

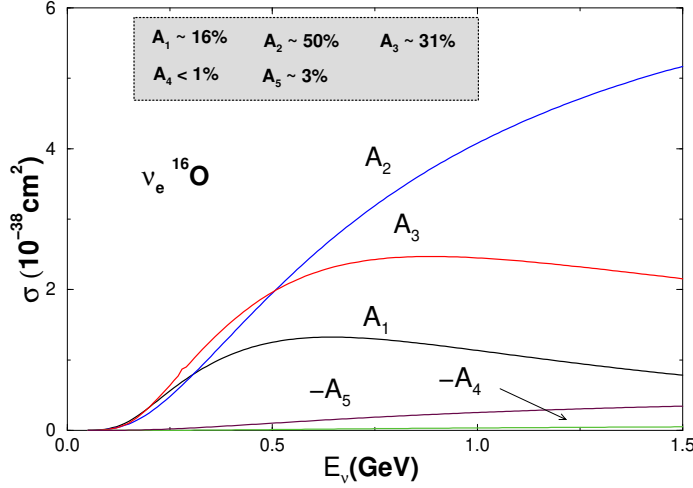


Fig. B.1. Contributions of the different structure functions, defined in Eq.(B.1), to the quasi-elastic process  $^{16}\text{O}(\text{e};\text{e}')\text{X}$ . The values given in the shaded box correspond to the areas under the different curves.

### C Form factors for quasi-elastic scattering

The hadronic current appearing in the definition of the hadronic tensor in Eq. (3) has the  $V - A$  structure  $J = J_V - J_A$ . The most general expressions of the vector and axial contributions read

$$J_V = J_V^+ = U(p^0) V^+ U(p) \\ J_A = J_V^+ = U(p^0) A^+ U(p) ;$$

where  $p$  ( $p^0$ ) are the momenta of the incoming (outgoing) nucleon and  $V$  and  $A$  are given by:

$$V = F_1 + i q \frac{F_2}{2m_N} + q F_S \\ A = 5 F_A + i 5 q F_T + q 5 F_P$$

In the definition of  $J_V$  and  $J_A$ ,  $+$  is the isospin raising operator acting on the isodoublet  $U = (n; p)^T$  and  $F_1; F_2; F_S; F_A; F_P; F_T$  are form factors depending on the squared four-momentum transfer  $q^2$ . The CVC hypothesis allows one to relate the weak form factors to the electromagnetic form factors and to constrain  $F_S(q^2) = 0$ . On the other hand, the PCAC hypothesis relates  $F_P(q^2)$  and  $F_A(q^2)$  in such a way that  $F_P(q^2) = 2m_N F_A(q^2) = (m^2 - q^2)$ . Finally, as a second class current is incompatible with the Standard Model of electroweak interactions [61], we set  $F_T(q^2) = 0$ .

To express the structure functions in terms of form factors we need to add the  $VV$ ,  $AV$  and  $AA$  contributions to the hadronic tensor (3) and equate the resulting sum to the decomposition (7). Thus, we obtain:

$$\begin{aligned}
 W_1 &= 2 \frac{q^2}{2} (F_1 + F_2)^2 + 2m_N^2 \frac{q^2}{2} F_A^2 \\
 W_2 &= 4 F_1^2 \frac{q^2}{4m_N^2} F_2^2 + F_A^2 \\
 W_3 &= 4 (F_1 + F_2) F_A \\
 W_4 &= 2 F_1 F_2 + 2m_N^2 + \frac{q^2}{2} \frac{F_2^2}{4m_N^2} + \frac{q^2}{2} F_P^2 - 2m_N F_P F_A \\
 W_5 &= \frac{W_2}{2} :
 \end{aligned}$$

Defining the electric ( $G_E$ ) and magnetic ( $G_M$ ) form factors

$$G_E = \frac{1}{1 - \frac{q^2}{M_V^2}} \quad G_M = 4.71 G_E ; \quad (C.1)$$

and  $q^2 = 4m_N^2$ , we finally get

$$\begin{aligned}
 F_1 &= \frac{1}{1 - (G_E + G_M)} \quad F_2 = \frac{1}{1 - (G_E + G_M)} \\
 F_A &= \frac{1.26}{1 - \frac{q^2}{M_A^2}} \quad F_P = \frac{1.28}{1 - \frac{q^2}{0.14}} \quad \frac{F_A}{1.27}
 \end{aligned}$$

## D Averaged cross sections

In Table (D.1) we show the results of for the  $QE$  and  $\bar{p}p$  production induced by neutrino and antineutrino, for the two-beam scenarios described in the paper.

## References

[1] Y. Fukuda et al. [Super-Kamiokande Collaboration], Phys. Rev. Lett. 81 (1998) 1562 [arXiv:hep-ex/9807003]; M. Ambrosio et al. [MACRO

		$QE (10^{-38} \text{ cm}^2)$	$(10^{-38} \text{ cm}^2)$
e	100	3.3	0.28
e	60	0.34	0.002
e	250	6.55	2.9
e	150	1.35	0.21

Table D.1

Average cross section (see Eq.(18)) for  $QE$  scattering and production induced by neutrino and antineutrino. The two different sets of values correspond to the fluxes shown in Fig. 1.

Collaboration], Phys. Lett. B 517 (2001) 59 [[arX iv:hep-ex/0106049](#)]; M. H. Ahn et al. [K2K Collaboration], Phys. Rev. Lett. 90 (2003) 041801 [[arX iv:hep-ex/0212007](#)]; B. T. Cleveland et al., Astrophys. J. 496 (1998) 505; J. N. Abdurashitov et al. [SAGE Collaboration], Phys. Rev. C 60 (1999) 055801 [[arX iv:astro-ph/9907113](#)]; W. Hampel et al. [GALLEX Collaboration], Phys. Lett. B 447 (1999) 127; S. Fukuda et al. [Super-Kamiokande Collaboration], Phys. Rev. Lett. 86 (2001) 5651 [[arX iv:hep-ex/0103032](#)]; Q. R. Ahmad et al. [SNO Collaboration], Phys. Rev. Lett. 87 (2001) 071301 [[arX iv:nucl-ex/0106015](#)]; K. Eguchi et al. [KamLAND Collaboration], Phys. Rev. Lett. 90 (2003) 021802 [[arX iv:hep-ex/0212021](#)].

- [2] C. Athanassopoulos et al. [LSND Collaboration], Phys. Rev. Lett. 81 (1998) 1774 [[arX iv:nucl-ex/9709006](#)]; A. Aguilar et al. [LSND Collaboration], Phys. Rev. D 64 (2001) 112007 [[arX iv:hep-ex/0104049](#)].
- [3] I. Stancu et al. [miniBooNE collaboration], FERMILAB-TM-2207.
- [4] B. Pontecorvo, Sov. Phys. JETP 6 (1957) 429 [Zh. Eksp. Teor. Fiz. 33 (1957) 549]; Z. Maki, M. Nakagawa and S. Sakata, Prog. Theor. Phys. 28 (1962) 870; B. Pontecorvo, Sov. Phys. JETP 26 (1968) 984 [Zh. Eksp. Teor. Fiz. 53 (1967) 1717]; V. N. Gribov and B. Pontecorvo, Phys. Lett. B 28 (1969) 493.
- [5] M. Apollonio et al. [CHOOZ Collaboration], Phys. Lett. B 466 (1999) 415 [[arX iv:hep-ex/9907037](#)]; Eur. Phys. J. C 27 (2003) 331 [[arX iv:hep-ex/0301017](#)].
- [6] S. Goswami, A. Bandyopadhyay and S. Choubey, Nucl. Phys. Proc. Suppl. 143, 121 (2005) [[arX iv:hep-ph/0409224](#)].
- [7] M. C. Gonzalez-Garcia, Phys. Scripta T 121, 72 (2005) [[arX iv:hep-ph/0410030](#)].
- [8] S. N. Ahmed et al. [SNO Collaboration], Phys. Rev. Lett. 92 (2004) 181301 [[arX iv:nucl-ex/0309004](#)].
- [9] A. Cervera, A. Donini, M. B. Gavela, J. J. Gomez Cadenas, P. Hernandez, O. Mena and S. Rigolin, Nucl. Phys. B 579 (2000) 17 [Erratum -ibid. B 593 (2001) 731] [[arX iv:hep-ph/0002108](#)].

[10] A. Donini, D. Meloni and P. Migliozzi, *Nucl. Phys. B* 646 (2002) 321 [[arX iv:hep-ph/0206034](#)];  
 D. Autiero et al., *Eur. Phys. J. C* 33 (2004) 243 [[arX iv:hep-ph/0305185](#)].

[11] J. Burguet-Castell, M. B. Gavela, J. J. Gomez-Cadenas, P. Hernandez and O. Medina, *Nucl. Phys. B* 608 (2001) 301 [[arX iv:hep-ph/0103258](#)];  
 J. Burguet-Castell and O. Medina, [arX iv:hep-ph/0108109](#).

[12] V. Barger, D. Marfatia and K. Whisnant, *Phys. Rev. D* 65 (2002) 073023 [[arX iv:hep-ph/0112119](#)].

[13] A. Donini, D. Meloni and S. Rigolin, *Eur. Phys. J. C* 45, 73 (2006) [[arX iv:hep-ph/0506100](#)].

[14] Y. Itow et al., [arX iv:hep-ex/0106019](#).

[15] P. Zucchelli, *Phys. Lett. B* 532 (2002) 166.

[16] S. Geer, *Phys. Rev. D* 57 (1998) 6989 [Erratum *ibid. D* 59 (1999) 039903] [[arX iv:hep-ph/9712290](#)]; A. De Rujula, M. B. Gavela and P. Hernandez, *Nucl. Phys. B* 547 (1999) 21 [[arX iv:hep-ph/9811390](#)].

[17] S. Manly, talk given at "8th International Workshop on Neutrino Factories, Superbeams and Betabeams", University of California, Irvine August 24-30, 2006.

[18] H. Tanaka, talk given at "8th International Workshop on Neutrino Factories, Superbeams and Betabeams", University of California, Irvine August 24-30, 2006.

[19] J. Bouchez, M. Lindroos and M. Mazzetto, *AIIP Conf. Proc.* 721, 37 (2004) [[arX iv:hep-ex/0310059](#)].

[20] J. Burguet-Castell, D. Casper, J. J. Gomez-Cadenas, P. Hernandez and F. Sanchez, [arX iv:hep-ph/0312068](#).

[21] A. Donini, E. Fernandez-Martinez, P. Migliozzi, S. Rigolin and L. Scotto Lavina, *Nucl. Phys. B* 710, 402 (2005) [[arX iv:hep-ph/0406132](#)].

[22] D. Casper, *Nucl. Phys. Proc. Suppl.* 112, 161 (2002).

[23] H. Gallagher, *Nucl. Phys. Proc. Suppl.* 112, 188 (2002).

[24] Y. Hayato, *Nucl. Phys. Proc. Suppl.* 112, 171 (2002).

[25] Modern Topics in Electron Scattering, Eds. B. Frois and I. Sick (World Scientific, Singapore, 1991).

[26] O. Benhar, V.R. Pandharipande and S.C. Pieper, *Rev. Mod. Phys.* 65, 817 (1993).

[27] O. Benhar, N. Farina, H. Nakamura, M. Sakuda and R. Seki, *Phys. Rev. D* 72, 053005 (2005) [[arX iv:hep-ph/0506116](#)].

[28] R. A. Smith and E. J. Moniz, *Nucl. Phys. B* 43 (1972) 605 [Erratum *ibid. B* 101 (1975) 547]; E. J. Moniz, *Phys. Rev.* 184, 1154 (1969).

[29] E. J. Moniz, I. Sick, R. R. Whitney, J. R. Ficenec, R. D. Kephart and W. P. Trower, *Phys. Rev. Lett.* 26 (1971) 445.

[30] F. A. Briesa and A. Della Gre, *Nucl. Phys. A* 292 (1977) 445; H. Nakamura and R. Seki, *Nucl. Phys. Proc. Suppl.* 112 (2002) 197.

[31] Omer Benhar, *Nucl. Phys. B (Proc. Suppl.)* 139 (2005) 15.

[32] G. J. Kramer, H. P. Block and L. Lapikas, *Nucl. Phys. A* 679 (2001) 267.

[33] D. Rohe, et al, *Phys. Rev. Lett.* 93 (2004) 182501.

[34] R. B. Warringa, V. G. J. Stoks, R. Schiavilla, *Phys. Rev. C* 51, 38 (1995).

[35] S. C. Pieper and R. B. Warringa, *Ann. Rev. Nucl. Part. Sci.* 51, 53 (2001).

[36] A. E. L. D. Pieperink, T. de Forest and I. Sick, *Phys. Lett. B* 63, 261 (1976).

[37] C. Ciocegliatti, E. Pace and G. Salmè, *Phys. Rev. C* 21, 805 (1980).

[38] H. M. Eier-Hajduk, Ch. Hadjik and P. J. Sauer, *Nucl. Phys. A* 395, 332 (1983).

[39] C. Ciocegliatti, S. Liuti and S. Simula, *Phys. Rev. C* 41, R2474 (1990).

[40] H. Morita and T. Suzuki, *Prog. Theor. Phys.* 86, 671 (1991).

[41] O. Benhar and V. R. Pandharipande, *Phys. Rev. C* 47, 2218 (1993).

[42] O. Benhar, A. Fabrocini and S. Fantoni, *Nucl. Phys. A* 505, 267 (1989).

[43] A. Ramos, A. Polls and W. H. Dickho, *Nucl. Phys. A* 503, 1 (1989).

[44] O. Benhar, A. Fabrocini, S. Fantoni and I. Sick, *Nucl. Phys. A* 579, 493 (1994).

[45] Proceedings of NuInt01, Eds. J. G. Moron, M. Sakuda and Y. Suzuki, *Nucl. Phys. B (Proc. Suppl.)* 112 (2002); Proceedings of NuInt04, Eds. F. Cavanna, P. Lipari, C. Kappel and M. Sakuda, *Nucl. Phys. B (Proc. Suppl.)* 139 (2005).

[46] J. Serrau and C. Volpe, *Phys. Rev. C* 70, 055502 (2004) [[arXiv:hep-ph/0403293](https://arxiv.org/abs/hep-ph/0403293)].

[47] J. E. Amaro, J. Nieves and M. Valverde, *Phys. Rev. C* 70, 055503 (2004) [Erratum *ibid. C* 72, 019902 (2005)] [[arXiv:nucl-th/0408005](https://arxiv.org/abs/nucl-th/0408005)].

[48] S. Ahmad, M. Sajjad Athar and S. K. Singh, [nucl-th/0603001](https://arxiv.org/abs/nucl-th/0603001).

[49] J. A. Caballero, C. M. Alberon, M. C. Martínez and J. M. Udías, *Phys. Rev. C* 68, 048501 (2003) [[arXiv:nucl-th/0303075](https://arxiv.org/abs/nucl-th/0303075)].

[50] Y. Horikawa, F. Lenz, N. Maimai Mukhopadhyay, *Phys. Rev. C* 22 (1980) 1680.

[51] O. Lalakulich and E. A. Paschos, *Phys. Rev. D* 71, 074003 (2005).

[52] O. Benhar and D. Meloni, [hep-ph/0604071](https://arxiv.org/abs/hep-ph/0604071). *Phys. Rev. Lett.*, in press.

[53] H .N akam ura and R .Seki, Nucl. Phys. B (Proc. Suppl) 112, 197 (2002).

[54] B .Szczerbinska, T .Sato, K .Kubodera, T .S H .Lee, nucl-th/0610093.

[55] O .Lalakulich, E A .Paschos and G .P iranishvili Phys. Rev. D 74, 014009 (2006).

[56] S .Ahmad, M .Sajjad Athar and S.K .Singh, nucl-th/0601045.

[57] T .Leitner, L .A lvarez-Ruso and U .M osel, Phys. Rev. C 73, 065502 (2006) [arX iv:nucl-th/0601103].

[58] M .O .Wascko [in]BoNE Collaboration]. arX iv:hep-ex/0602050.

[59] H .N akam ura, talk given at "8th International Workshop on Neutrino Factories, Superbeams and Betabeams", University of California, Irvine August 24-30, 2006.

[60] J.J .Gomez Cadenas and M .Wascko, private communications.

[61] T D .Lee, Particle physics and Introduction to Field Theory, Harwood, Chur, 1988.